An Experimental Investigation of the Mixing of Coannular Swirling Flows

Jack D. Mattingly* and Gordon C. Oates†
University of Washington, Seattle, Washington

An extensive investigation of the mixing behavior of coannular streams, with swirl present, has been carried out. A large blowdown facility was adapted to provide two streams of air at variable stagnation pressures but equal stagnation temperatures. Conditions within the mixing region were essentially incompressible. The facility was constructed to provide swirl in the inner stream, and a fixed inner and outer annulus could be provided if desired. In all cases considered, swirl was present in the inner but not the outer stream, thereby leading to flow conditions unstable to the Rayleigh instability. Mean flow measurements only were obtained. A five-hole probe was used to obtain the static pressure, stagnation pressure, and three velocity components. Additional measurements included sidewall pressure measurements on the inner and outer annuli, as well as stream mass flow rates obtained from orifice plate meters. A variety of flow regimes were considered, including some without separated regions present. Where possible, the results were compared to the somewhat limited data available in the literature.

Introduction

THE turbulent mixing of flows with significant streamline curvature is of interest in many environments of engineering interest. Bradshaw, in an extensive study,[1] considered the effects on the turbulence production rate of streamline curvature, including both longitudinal and lateral curvature. When confined flows are considered, strong interaction effects occur, in that the changed levels of turbulence encountered alter the mixing rates, which in turn significantly alter the fluid pressure gradients; hence, both the streamline curvature and turbulence production are affected. King, Rothfus, and Kermode[2] classified contained swirling flows according to the wall boundary conditions into the following types:

1) Unconfined swirling flows in which the wall effects are negligible (e.g., wake behind propeller or windmill).

2) Small length-to-diameter confined swirling flows, which occur in large-diameter chambers where sidewall effects strongly interact with the swirl to produce significant secondary reverse flows (e.g., combustors).

3) Large length-to-diameter confined swirling flows, which occur in tubes where circumferential wall effects interact strongly with the swirl flow (e.g., tubes of heat exchanger).

The third class of flows are considered in this study, both because, in cases without reverse flow regions, such flows are relatively simple and because there are examples of engineering interest in which such flow conditions may be employed directly to enhance engineering performance. Example possible engineering benefits to follow from exploitation of curved streamline effects include the use of curvature to introduce the Rayleigh instability[3] to enhance heat transfer (in heat exchangers), to enhance or control heat transfer and burning rates in solid fueled ramjets, or to enhance mixing in aircraft engine core stream-fan stream mixers. Analogous engineering benefits follow by exploiting the stabilizing influence of curvature in a flowfield with outwardly increasing angular momentum for environments where it is desired to reduce mass, momentum, or energy transport.

An effort was made in the present study to create some flows which though existing with strongly destabilizing curvature, would not introduce large regions of reverse flow. The hope was to provide sufficient detailed flow measurements to furnish useful information on mixing rates in a flowfield that was not so complex as to preclude computational verification. In this sense the study is somewhat analogous to that of Castro and Bradshaw[4] except that, in the case considered in Ref. 4, the streamline curvature was stabilizing to turbulence production. In addition, only mean flow properties were measured in the present study whereas turbulence properties were measured directly in Ref. 4.

It is to be noted that Gibson and Rodi[5] successfully reproduced the major features of the flowfield investigated in Ref. 4 by invoking a Reynolds-stress closure model of turbulence in their calculational scheme. The authors of Ref. 5 point out that such a model captures the important influence of the nonisotropy of the turbulence properties, a capability vital to describing the behavior of highly curved turbulent fields. It is to be noted further that conventional k-ϵ models do not have this capability.

It is hoped that the measurements reported herein will provide a further test for computational codes.

Experimental Procedure

Test Apparatus

The test apparatus can be considered to be composed of five major elements:

1) High pressure dual air supply system.
2) Concentric dual plenum section.
3) Swirl generator and nozzles section.
4) Test section.
5) Measurement system.

Figure 1 is a schematic diagram of the high-pressure air supply system. The system was adapted from the high-pressure supply system already in place in the University of Washington Aeronautical Laboratory (UWAL), which itself had been installed for the purpose of providing high-pressure air for propulsion simulation purposes. The system incorporates one high-pressure regulator, which pressurizes the two downstream lines to up to 600 psia. The separate stream

Presented as Paper 85-0186 at the AIAA 23rd Aerospace Sciences Meeting, Reno, NV, Jan. 14-17, 1985; received Feb. 4, 1985; revision received Aug. 21, 1985.

*Graduate Student; presently Associate Professor, Department of Aeronautics, USAF Academy, CO. Member AIAA.

†Professor, Department of Aeronautics and Astronautics. Associate Fellow AIAA.

flow rates are determined by installation of an appropriate choked orifice plate in each line. Subsequently, the air is expanded into the concentric dual plenum section (Fig. 2) where, after encountering "core busters," it passes through several sets of screens and honeycombs.

The air next passes through the swirl generator and nozzles section, where the inner stream passes through a row of stationary swirl vanes and both streams are accelerated to entry of the test section. The flow is introduced radially in a 1-in.-high passage. The swirl vane set consists of 20 adjustable stator vanes. The radius of the blade pivot shafts is 7 in., the blade chords are 2.32 in., and the blade spacing at the pivot shaft radius is 2.20 in. Each blade has a symmetric NACA 0024 shape about its radius, which is 2.75 in. These dimensions correspond to a blade camber of 50 deg. It is apparent that, especially with the imposed inward (radial) acceleration, the flow over the stator set is highly accelerating, and no evidence of substantial separation was found.

The measurement system is shown schematically in Fig. 3. Separate pressure transducers (Scan Co. PDCR22+1) are provided for all five ports of the five-hole probe, and many static pressure ports (18 ports on the upstream outside wall of the inner annulus, 28 ports on the downstream inner annulus, and 24 ports on the downstream outer annulus) are recorded through a two-transducer Scanivalve. Approximate

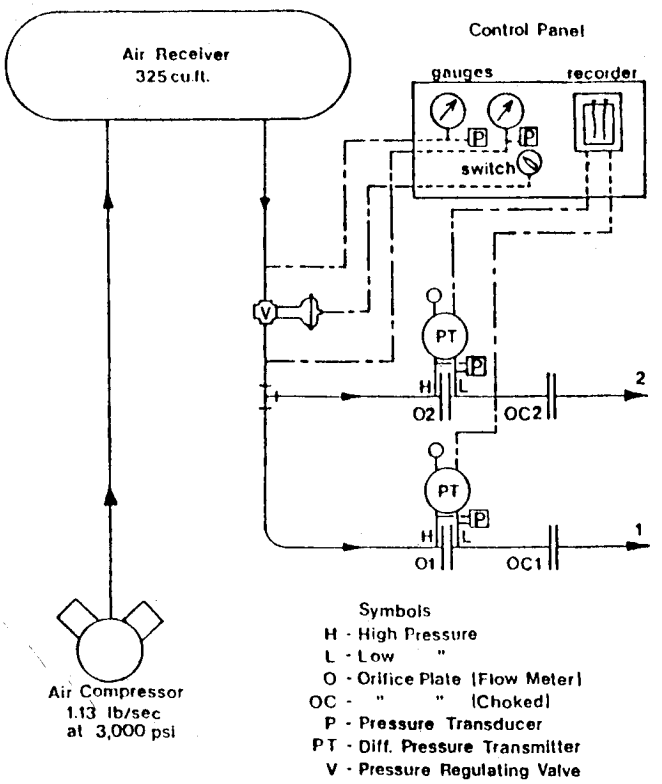

Fig. 1 High-pressure air supply system.

nulling of the angle of attack of the five-hole probe is achieved by nulling the differential pressure across ports 1 and 3 (Fig. 4) of the probe, as measured by a Statham transducer, No. PM283TC+0.15.

Five-Hole Probe

The sensor portion of the five-hole probes consists of a single forward hole positioned on the probe centerline, surrounded by four additional holes on the conical forebody (Fig. 4). Several small probes were constructed using the method suggested by Gallington and Hollenbaugh.[6] When the flow is contained by an outer annulus, as was the case for the results reported herein, the internal geometric restraints on probe configuration become severe. The design adopted by this study is shown in Fig. 5, where it can be seen that the probe is constructed to pass around the inner wall to measure properties in the annulus at the far side of the test section from the probe entry port.

Erwin[7] describes multihole probes and provides typical calibration data. The procedure described by Erwin requires accurate nulling of the probe, whereas such a procedure is inconvenient for use with the present facility because of the blowdown operation and geometric constraints. (At typical flow rates, run times were limited to about 10 min to avoid significant changes in the stagnation properties.) Dring et al.[8] describe a modified five-hole probe whose head remains in an essentially constant position when the probe is rotated. Such a probe was adapted for our use, so that, with the modified calibration procedure suggested by Barker et al.[9] to allow measurement at large flow angles, the high accuracy and limited time of measurement requirements could be met.

The probe calibration procedures are somewhat complex and must be conducted with care. A detailed description of calibration procedures and the related accuracies obtained are given in Ref. 10. It is to be noted that the probe was calibrated over a small range of angle of attack but over a substantial range of sideslip angles (± 50 deg). Inevitably, inaccuracies were encountered when such a wide sideslip angle range was considered; so, in order to improve the accuracy, two calibration ranges were utilized, $|\alpha| \leq 20$, $|\beta| \leq 10$ and $-50 \leq \alpha \leq -20$, $-6 \leq \beta \leq +8$. Thus, when measurement indicated that the magnitude of the sideslip angle was in excess of 20 deg, the coarse calibration was invoked, whereas the more accurate calibration was used for cases where the measured magnitude of the slideslip angle was less than 20 deg.

In common with all probes of this type, there are not yet reliable methods for calibrating the probe for the effects of large shear rates or of nearby solid surfaces. As a result, measurements taken near the solid boundaries, or within the early developing shear layer between streams, can only be interpreted qualitatively at best.

Once the calibration coefficients have been determined, the measured values of the pressures p_1 through p_5 yield a value for each of the following quantities: 1) axial velocity w, 2) tangential velocity v, 3) radial velocity u, 4) total velocity V, 5) static pressure p_s, and 6) stagnation pressure p_T.

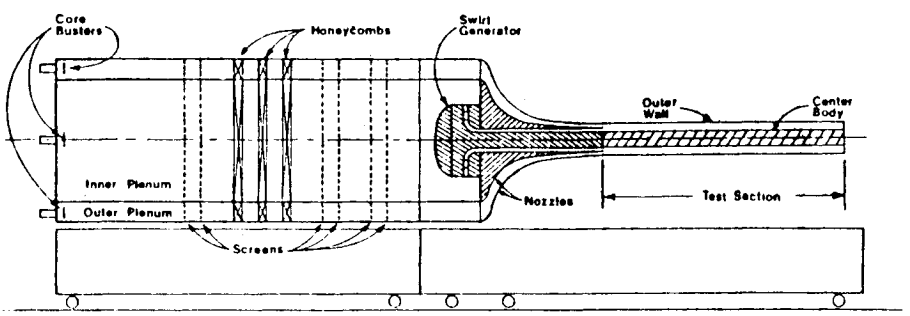

Fig. 2 Test apparatus.

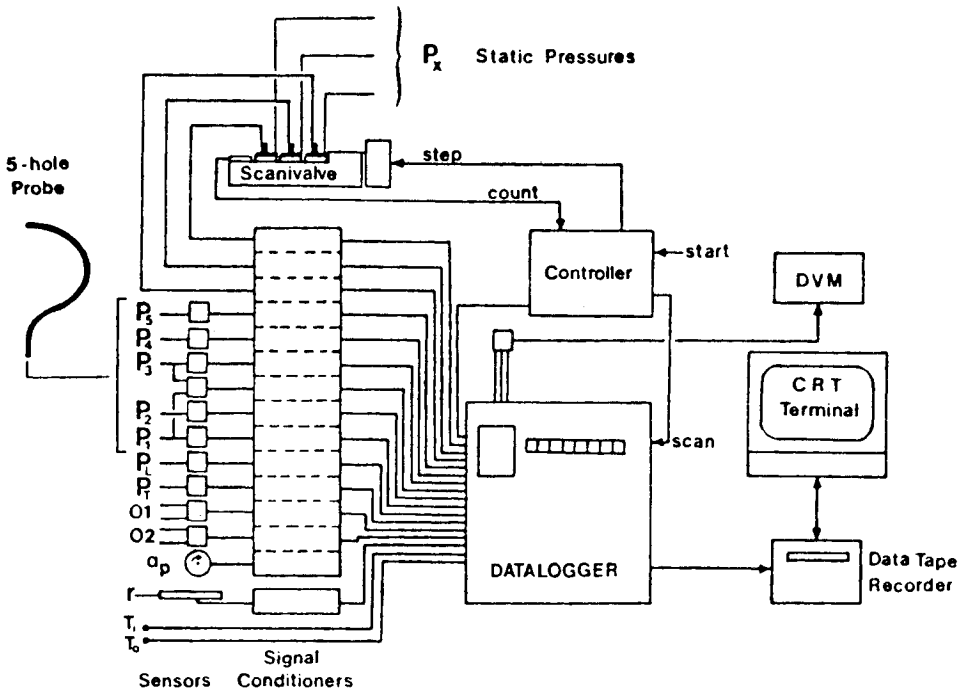

Fig. 3 Measurement system.

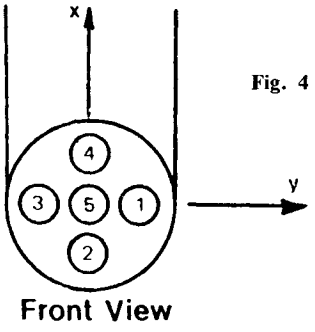

Fig. 4 Five-hole probe port numbering.

Configurations Tested

Four sets of experiments were considered in the parent study[10] to that reported here. The first three sets of experiments were run without the test section outer annulus present and involved these configurations: 1) swirling flow only exhausting into quiescent atmosphere, 2) swirling stream and surrounding axially directed stream exhausting into quiescent atmosphere, and 3) swirling stream and axially directed stream exhausting into quiescent atmosphere with test section inner annulus installed.

In this paper we consider only the results of the fourth set of experiments, in which the swirling inner stream and axially directed outer stream exhausted into the confined constant area test section depicted in Fig. 2. Five separate runs are considered, with parameters as summarized in Table 1. The parameters were varied by placing appropriately sized orifice plates at the choked orifice locations (Fig. 1) of the separate streams. The swirl generator was kept at the same geometric swirl angle for all runs, and the swirl parameter S was determined from measurements at the downstream location $z=0.25$ in.

Definitions

In order to characterize the magnitude of the "swirl" of a given flowfield, it is customary to define a swirl number as the ratio of the flow angular momentum to an appropriate flow axial momentum times a radius. To this end, consider the axisymmetric cylindrical coordinate form of the tangen-

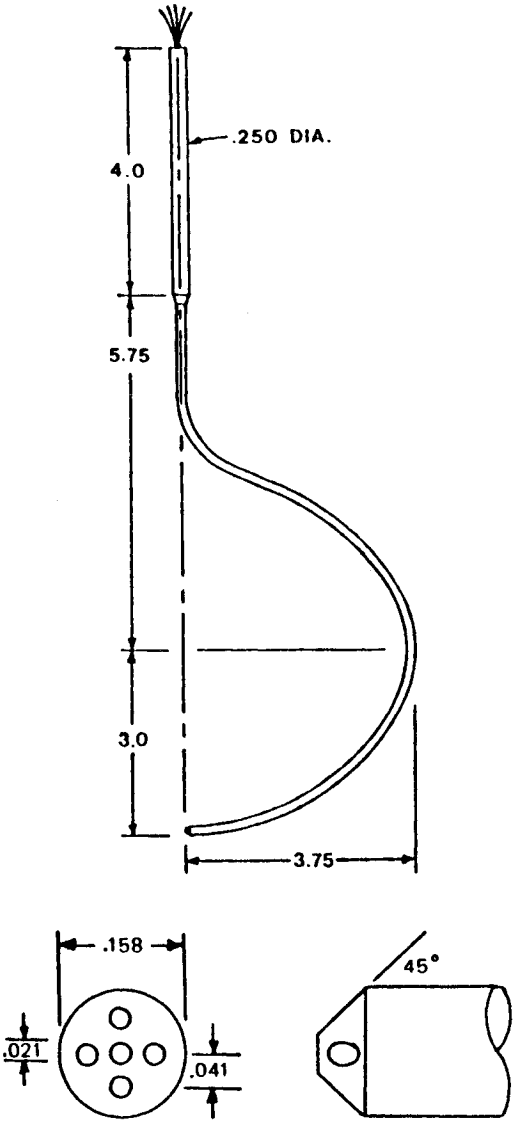

Fig. 5 Dimensions of probe in inches.

tial momentum equation, which may be written

$$ru\frac{\partial rv}{\partial r}+rw\frac{\partial rv}{\partial z}=\frac{1}{\rho}\frac{\partial r^2\tau_\Theta}{\partial r}$$

This may be expressed in conservative form by adding the continuity equation multiplied by rv to give

$$\frac{\partial r^2uv}{\partial r}+\frac{\partial r^2vw}{\partial z}=\frac{1}{\rho}\frac{\partial r^2\tau_\Theta}{\partial r}$$

Noting the no-slip boundary conditions at inner and outer radii, integration gives

$$\frac{dG_\Theta}{dz}=r^2\tau_\Theta\Big|_{r_i}^{r_o}$$

where $G_\Theta=\int_{r_i}^{r_o}\rho r^2wv\,dr$, τ_Θ = tangential component of shear stress, and r_o, r_i = test section outer and inner radii, respectively.

This expression simply expresses that the rate of change of angular momentum is equal to the net torque provided by the bounding walls. It does not, of course, provide any information concerning the internal distribution of the angular momentum. In this investigation, the angular momentum was obtained from measured values of the fluid properties as obtained in a flow traverse taken at the first station within the test section ($z=0.25$ in.).

An appropriate representation of the axial momentum follows by considering the axial momentum equation. Thus, the conservative form of the equation may be written

$$\frac{\partial uwr^2}{\partial r}+\frac{\partial w^2r^2}{\partial z}=-\frac{r}{\rho}\frac{\partial p}{\partial z}+\frac{1}{\rho}\frac{\partial r\tau_z}{\partial r}$$

Then, again noting the no-slip boundary condition and, in addition, restricting our attention to the case of constant radius annuli, integration gives

$$\frac{d}{dz}\left[\int_{r_i}^{r_o}(p-p_0+\rho w^2)r\,dr\right]=r\tau_z\Big|_{r_i}^{r_o}$$

In this expression, p_0 is an appropriate reference pressure, which in this investigation is taken as the static pressure measured at the outer wall of the inner stream at the location $z=-2$ in.

The integral in this last equation is in an awkward form to measure directly because of the presence of the static pressure, but a more convenient form is obtained by integration by parts. Thus,

$$\int_{r_i}^{r_o}(p-p_0+\rho w^2)r\,dr=G_z+\tfrac{1}{2}\left[(p_{r_o}-p_0)r_o^2-(p_{r_i}-p_0)r_i^2\right]$$

where

$$G_z=\int_{r_i}^{r_o}\rho(w^2-v^2/2)r\,dr$$

Note that the radial momentum equation

$$\frac{\partial p}{\partial r}\simeq\rho\frac{v^2}{r}$$

has been incorporated to obtain this expression. The swirl number S is now defined as

$$S=G_\Theta\Big/r_o\int_{r_i}^{r_o}(p-p_0+\rho w^2)r\,dr$$

Table 1 Test run parameters

Run no.	Mass flow ratio, α	$\bar{w}_o/\bar{w}_i$	Swirl no. S
1	0.00	0.000	0.1762
2	0.47	0.336	0.9579
3	1.00	0.714	0.1096
4	2.13	1.512	0.0379
5	3.91	2.793	0.0125

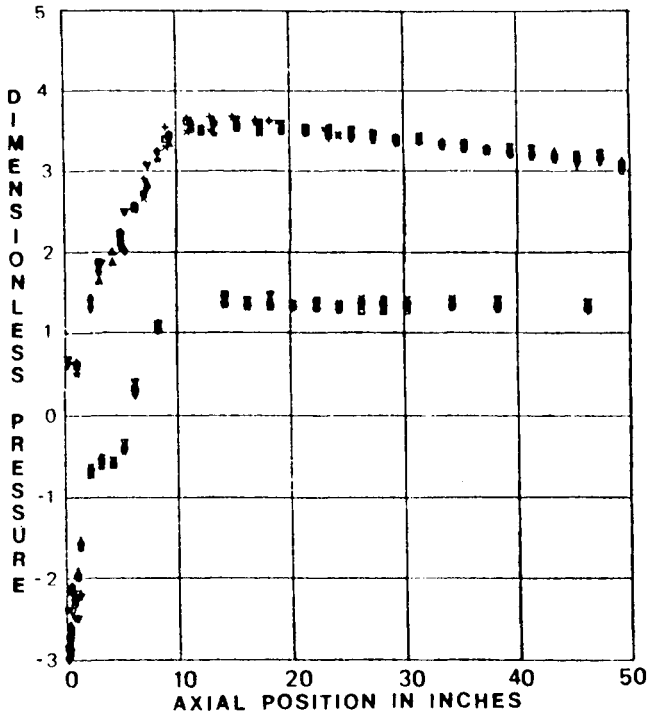

Fig. 6 Static pressures on 4- and 8-in. tubes, run 1.

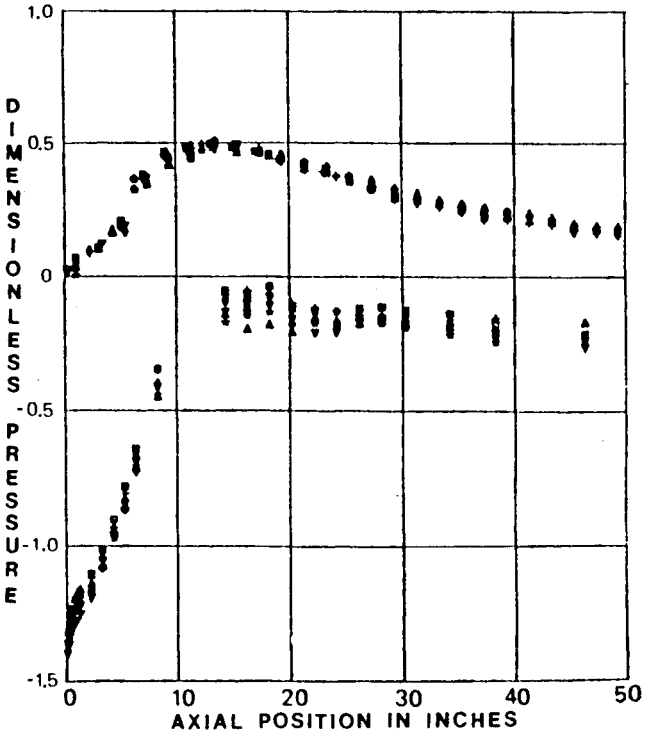

Fig. 7 Static pressures on 4- and 8-in. tubes, run 2.

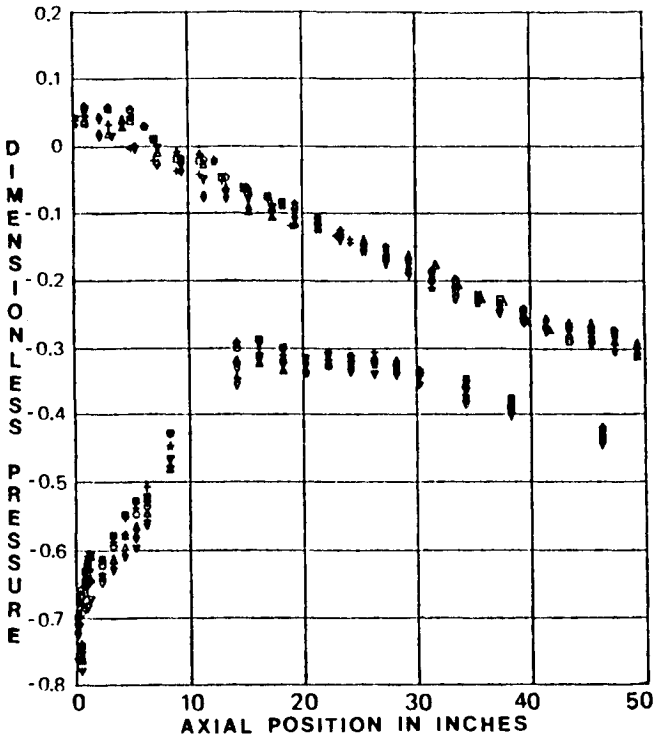

Fig. 8 Static pressures on 4- and 8-in. tubes, run 3.

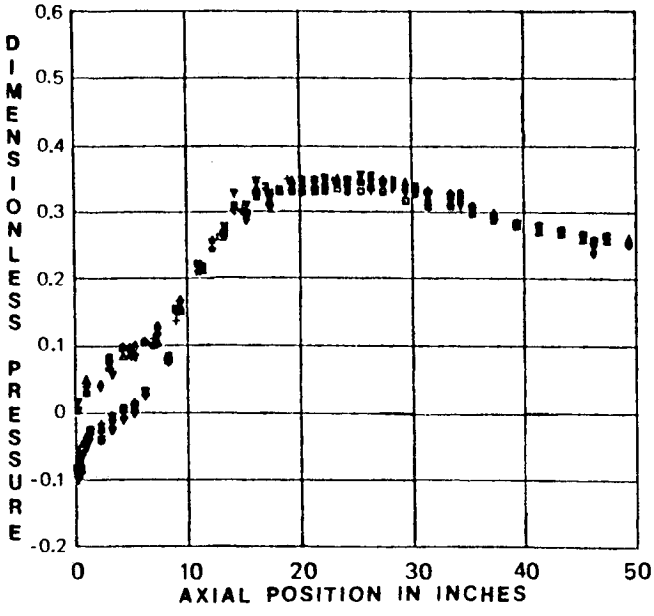

Fig. 9 Static pressures on 4- and 8-in. tubes, run 5.

or

$$S=\frac{G_\Theta}{r_o G_z+(r_o/2)[p_{r_o}-p_0)r_o^2-(p_{r_i}-p_0)r_i^2]}$$

This form of the swirl number can be evaluated directly from the measurements, and it is apparent from the manipulations leading to the expression that, except for the effects of surface friction, S will be a constant throughout the test section.

Results of the Experiments

Static Pressure Variation

The static pressures on the inner and outer annuli are shown in Figs. 6-9. The measurements reveal the

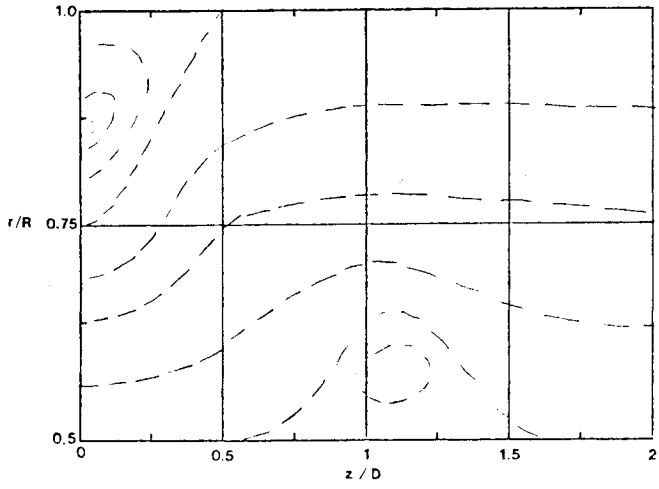

Fig. 10 Streamline pattern for run 1.

"integrated" effects of rather complex interactions. Thus, if the mixing of nonswirling flows is considered, the faster of the two streams tends to transfer momentum to the slower via turbulent mixing. Any diffusion of the faster stream, however, introduces an adverse pressure gradient that tends to separate the slower stream. This competition between turbulent momentum transfer and imposed pressure gradient momentum reduction is further complicated by the addition of swirl. The outward shift of angular momentum leads to a reduction in the pressure difference between inner and outer annuli (because of the related reduction in radial pressure gradient). This reduced pressure difference effectively imposes an additional favorable pressure gradient on the outer wall and an additional adverse pressure gradient on the inner wall. When all these effects are combined with the conventional favorable pressure gradient created by the wall shear stresses, interpretation is complex indeed.

Run 1, Fig. 6, leads to perhaps the most complex flowfield of all. The sudden expansion of the swirling jet into the outer (nonflowing) stream leads to very energetic mixing of the swirling stream, and the resultant sudden expansion of the inner stream leads to a pronounced region of separation. The pressure signatures evident in Fig. 6 indicate the probable presence of separation, particularly the pronounced plateau evident on the inner wall at approximately 5 in. A detailed survey of the flowfield supports the implications of the sidewall pressure measurements where, as shown in Fig. 10, the flow is found to separate on the inner annulus. Following reattachment, both inner and outer surface pressures decrease with axial distance as expected. It is apparent from the slow rate at which the two pressures approach each other that the aggravated mixing near the entrance succeeds in substantially redistributing the angular momentum, with subsequent swirl reduction reflecting the actual reduction of angular momentum due to surface friction forces. In this respect it is well to keep in mind when interpreting the figures that the static pressures are nondimensional with respect to the dynamic pressure of the flow based on average axial velocity. That is,

$$\text{dimensionless pressure}=\frac{p-p_0}{\frac{1}{2}\rho\bar{w}^2}$$

where $\bar{w}$ = mass average axial velocity and p_0 = reference pressure at outer wall of inner stream at $z=-2$ in. (as previously defined).

The authors elected not to present further detailed measurements obtained for case 1 because of the emphasis on the simpler cases in which reverse flow did not appear. The partial results of Figs. 6 and 10, however, agree in

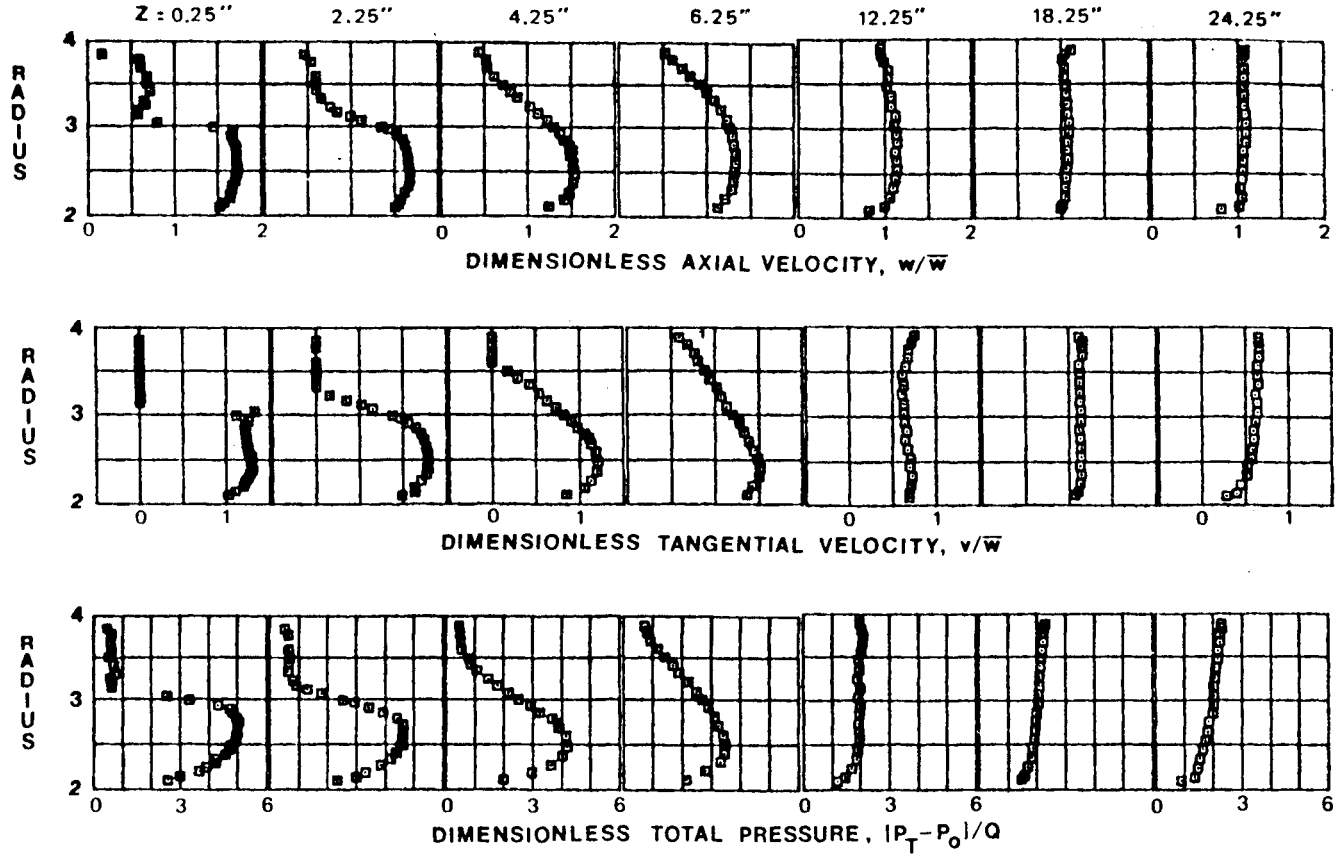

Fig. 11 Typical flowfield properties, run 2.

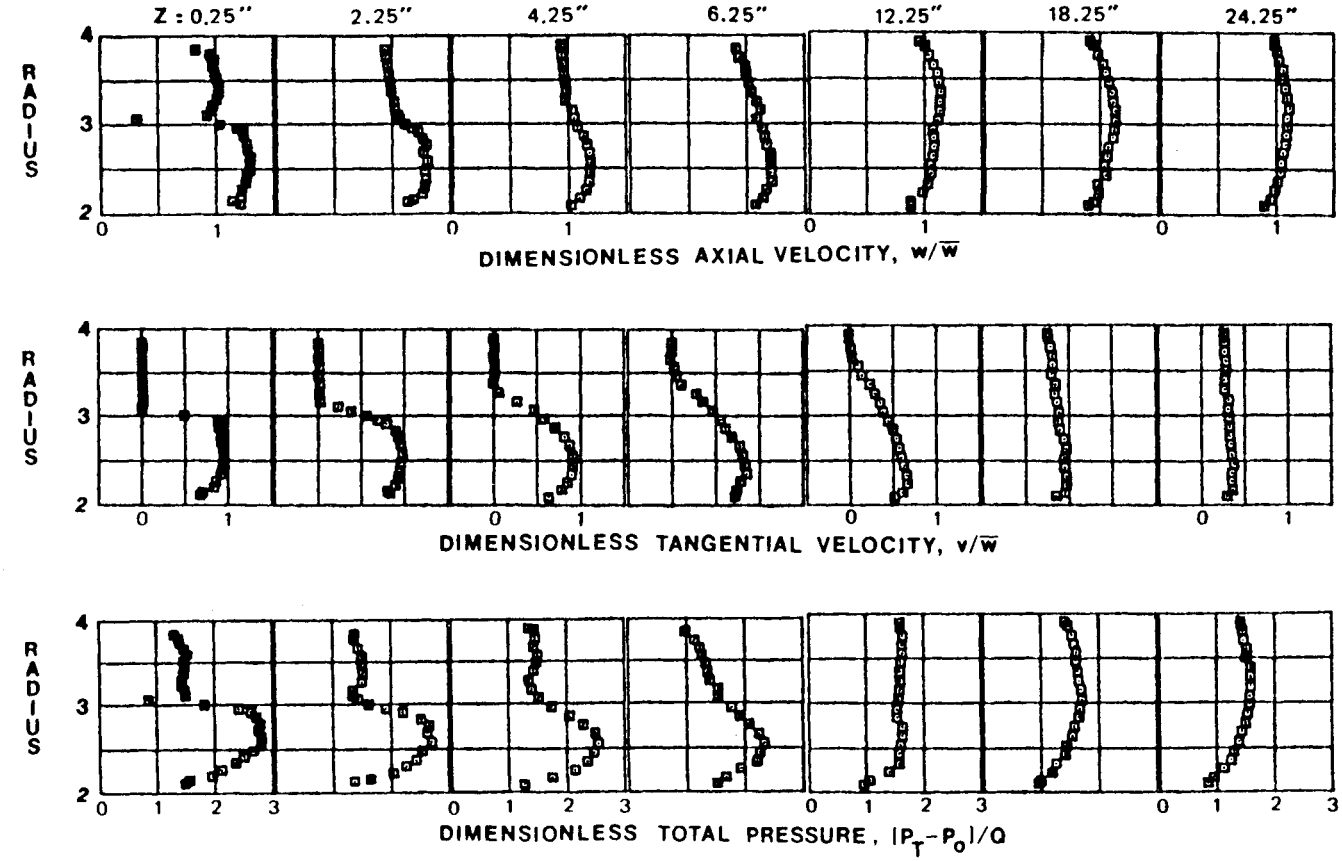

Fig. 12 Typical flowfield properties, run 2.

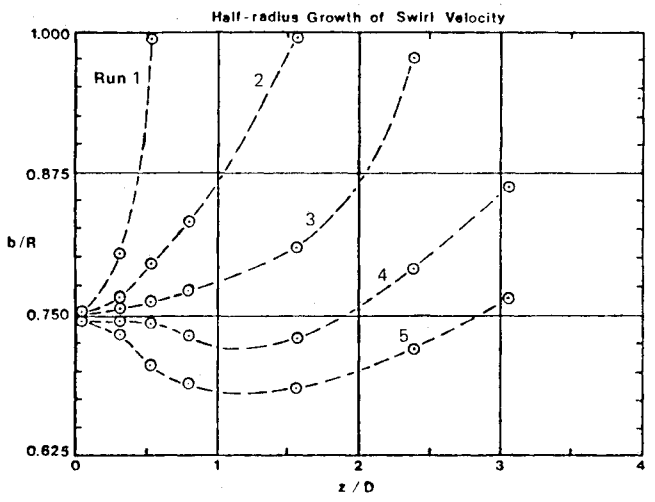

Fig. 13 Half-radius growth of swirl velocity.

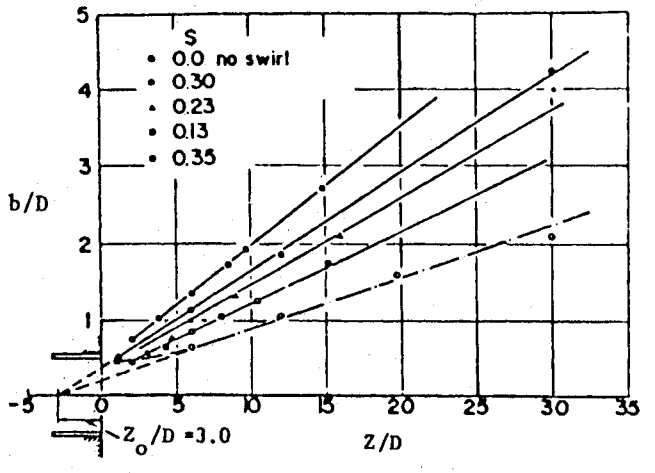

Fig. 14 Half-radius growth as a function of swirl number for swirling freejet (Ref. 12).

qualitative tendencies with measurements such as those provided in Ref. 11, where the investigation was directed to flows in which separation and the resulting substantial effects of longitudinal curvature played a significant role.

Figure 7 reveals that the introduction of some flow in the outer stream (case 2, $\alpha = 0.47$) has a pronounced effect on the pressure distributions, with the initial adverse pressure gradient being much reduced on both the inner and outer walls. No separation was detected in either the sidewall pressure measurements or in the five-hole probe traverses. The effect of the initial rapid outward convection of the angular momentum is evident in the initial rapid decrease in pressure difference between inner and outer walls. Subsequently, both inner and outer surface pressures decrease with only a gradual reduction of the difference in wall pressures.

As the outer stream mass flow rate is further increased (case 3, Fig. 8), the tendencies evidenced are as expected from qualitative reasoning. Thus, because of the increasing momentum of the outer stream, the effect of the inner stream on the outer pressure distribution is not as pronounced as in the lower flow rate cases. As with all the cases considered, however, the difference of the wall pressures reflects an initial rapid redistribution of the momentum contained within the inner stream, followed by the gradual decay of the overall momentum contained within the stream.

The results of case 5, illustrated in Fig. 9, indicate that the now highly energetic external stream is behaving very nearly as if it is expanding into a sudden expansion with no flow in the internal stream.

Behavior of Velocities and Stagnation Pressures

Extensive sets of flowfield properties were obtained, and typical results are depicted in Figs. 11 and 12. It is evident in both sets of figures that the enhanced mixing rate caused by the presence of the swirl in the inner stream leads to rapid outward migration of the angular momentum and rapid mixing out of the stagnation pressure profile.

The detailed data of Figs. 11 and 12 are useful for quantitative comparisons, but interpretation of the flowfield interactions is aided by observation of the behavior of integral properties of the flowfield. In this respect, Fig. 13 displays the axial growth of the half-radius of the swirl velocity. (The half-radius is defined as the radius at which the tangential velocity is one-half the maximum tangential velocity.) As described earlier in the section "Configurations Tested," all runs described herein were obtained with the swirl generator set at a fixed angle. Variation of the momentum of the external stream, then, really varies two important ratios: the ratio of the magnitude of the axial velocity of the outer stream to the angular momentum and the ratio of the axial momenta for the two streams. The results follow predictable trends in that an increasing swirl number leads to sharply increased growth of the swirl velocity half-radius. Increasing the ratio of outer to inner momentum leads to the inward transfer of axial momentum, contracting the inner stream to such an extent that the outward transfer of tangential momentum is overcome from the point of view of the radial position migration (but not from the point of view of stream function migration).

The authors of this report have had little success locating results for quantitative comparison, but qualitative similarities with the results presented here are shown in Figs. 14 and 15. Figure 14, taken from Ref. 12, shows the variation of half-radius for a swirling freejet at several values of swirl number. This case is remotely comparable to case 1 considered herein, but it is evident that the pressure gradients generated by the containing outer annulus in the experiments reported herein lead to a more rapid half-swirl radius growth rate. The tendency to reduce outward migration of the half-swirl radius is illustrated in Fig. 15, taken from Ref. 13. Once again, though the results have tendencies somewhat similar to those presented herein, direct comparison is not warranted because of the different geometries considered.

As a final comparison of the behavior of an integral property, the axial variation of the swirl number for each of the five cases considered is shown in Fig. 16. It is to be noted that the swirl numbers depicted are nondimensionalized by the test section entry values. The decay of the swirl number represents a rather complex interaction, as it is clear that both the axial momentum contribution $\{\int_{r_i}^{r_o}(p-p_0+\rho w^2)r\,dr\}$ and angular momentum contribution G_θ tend to decrease in the axial direction. It is evident that for the higher swirl numbers the decay of G_θ dominates, particularly in the initial portions of the flow, where very large swirl velocities exist in the neighborhood of the inner annulus. In case 4, for which the axial momentum in the outer stream is very large, it is apparent that the viscous stresses on the outer annulus wall lead to an initially rapidly decreasing axial momentum contribution and hence increase in swirl number. Subsequently, the increasing decay of G_θ (probably brought about by the significant interaction of the angular momentum and outer wall) leads to a decreasing swirl number.

It is believed by the authors of this report that the results of run 5 are essentially anomalous. The very small swirl present, compared to overall axial flow, renders it difficult to measure the swirl number accurately particularly as the angular momentum becomes distributed among the high axial momentum, high-radius streamlines. This result is exacer-

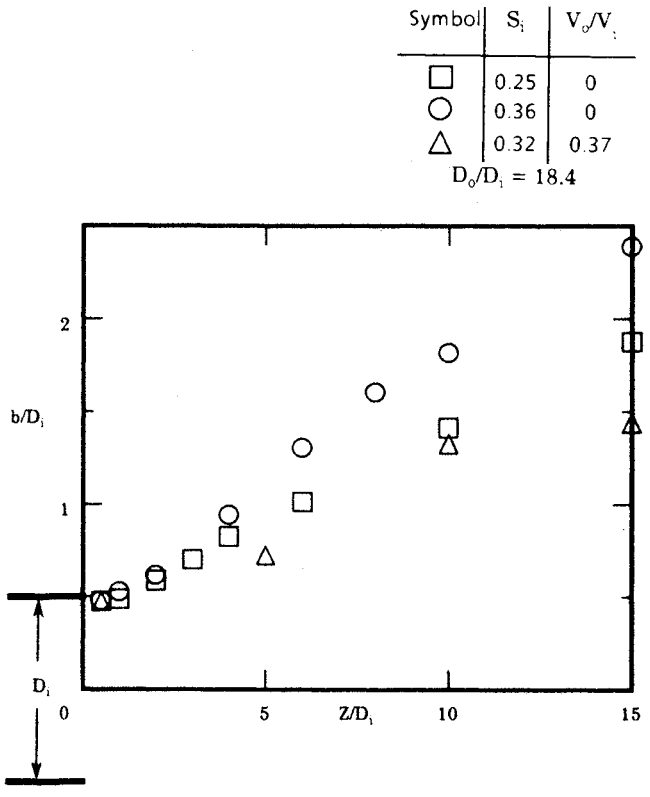

Fig. 15 Half-radius growth of swirl velocity for swirling jet with and without external stream (Ref. 13).

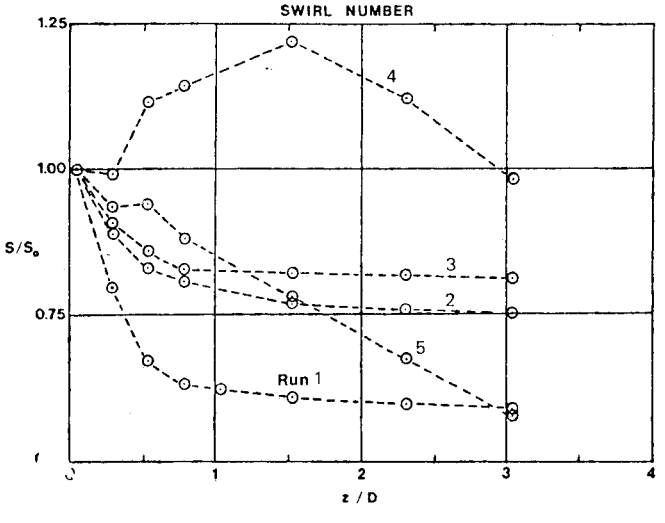

Fig. 16 Swirl number decay.

bated by the flow angles in the outer portion of the annulus requiring use of the coarse data reduction calibration and, hence, giving very coarse accuracies for such small swirl angles.

Summary and Conclusions

Experimental investigation of the flowfield resulting from the mixing of incompressible coannular airstreams with substantial swirl present in the inner stream revealed a number of important fluid dynamic phenomena. It is evident that enhanced radial mixing is created as a result of the Rayleigh instability, which itself is present because of the outwardly decreasing angular momentum of the fluid found in all cases considered herein.

The presence of a finite radius inner annulus prevented the occurrence of separated flows in all cases considered but one. However, the presence of the containing outer annulus ensured that any enhanced mixing would reflect also in substantial pressure variations, so that the problem considered must definitely be considered a strong interaction problem. An example of this latter concept appears in comparison to the growth rate of the swirl half-radius as measured in the present series with other investigators' data for the mixing of swirling freejets. In the cases considered herein, the generation of adverse pressure gradients leads to a substantially higher swirl half-radius growth rate.

Acknowledgment

The authors are indebted to the Air Force Office of Scientific Research for support under Grant AFOSR-80-0186G.

References

[1]Bradshaw, P., "Effects of Streamline Curvature on Turbulent Flow," AGARDograph 169, 1973.

[2]King, M. K., Rothfus, R. R., and Kermode, R. I., "Static Pressure and Velocity Profiles in Swirling Incompressible Tube Flow," *American Institute of Chemical Engineers Journal*, Vol. 15, Nov. 1969, pp. 837-842.

[3]Rayleigh, Lord, "On the Dynamics of Revolving Fluids," *Proceedings of the Royal Society of London*, Ser. A93, 1917, pp. 148-154.

[4]Castro, I. P. and Bradshaw, P., "Turbulence Structure of a Highly Curved Mixing Layer," *Journal of Fluid Mechanics*, Vol. 73, 1976, pp. 265-304.

[5]Gibson, M. M. and Rodi, W., "A Reynolds Stress Closure Model of Turbulence Applied to the Calculations of a Highly Curved Mixing Layer," *Journal of Fluid Mechanics*, Vol. 103, 1981, pp. 161-182.

[6]Gallington, R. W. and Hollenbaugh, C. F., "A Fast Method for Accurate Manufacture of Small Five-Hole Probes," *Aeronautics Digest*, Spring 1979; USAFA-TR-79-7, USAF Academy, CO, July 1979.

[7]Erwin, J. R., "Experimental Techniques," *Aero-dynamics of Turbines and Compressors, High Speed Aerodynamics and Jet Propulsion*, Vol. X, Sec. D, Princeton University Press, Princeton, 1964.

[8]Dring, R. P., Joslyn, H. D., and Hardin, L. W., "Experimental Investigation of Compressor Rotor Wakes," United Technologies Research Center, East Hartford, CT, Rept. AFAPL-TR-79-2107, Jan. 1980.

[9]Barker, K. R., Gallington, R., and Minster, S., "Calibration of Five-Hole Probes for on Line Data Reduction," *Aeronautics Digest*, Spring 1979; USAFA-TR-79-7, USAF Academy, CO, July 1979.

[10]Mattingly, J. D., "Experimental Investigation of the Mixing of Highly Swirling Flows," Ph.D. Dissertation, University of Washington, Seattle, 1982.

[11]Roback, R. and Johnson, B. V., "Mass and Momentum Turbulent Transport Experiments with Confined Swirling Coaxial Jets," NASA Contractor Rept. 168252, Aug. 1983.

[12]Pratte, B. D. and Rask, D. R., "Turbulent Viscosities for Swirling Flow in a Stationary Annulus," *Journal of Fluids Engineering, Trans. ASME*, Dec. 1973, pp. 557-566.

[13]Launder, B. E. and Morse, A., "Some Experiments on the Turbulent Swirling Jet with and without External Stream," Unpublished paper, London, England.